65

Workshop on Precision Manipulation at the Micro and Nano Scales, 1998 IEEE International Conference on Robotics and Automation, Leuven, Belgium, May 16-20, 1998.

Assembly Planning at the Micro Scale

John T. Feddema, Patrick Xavier, Russell Brown
Sandia National Laboratories[1]
P.O. Box 5800, MS 1003
Albuquerque, NM 87185

Abstract

This paper investigates a new aspect of fine motion planning for the micro-domain. As parts approach 1-10 μm or less in outside dimensions, interactive forces such as van der Waals and electrostatic forces become major factors which greatly change the assembly sequence and path plans. It has been experimentally shown [1][2] that assembly plans in the micro-domain are not reversible, motions required to pick up a part are not the reverse of motions required to release a part. This paper develops the mathematics required to determine the goal regions for pick up, holding, and release of a micro-sphere being handled by a rectangular tool.

1. Introduction

In recent years, the world economy has seen expansive market growth in the area of MEMS (Micro-Electro-Mechanical Systems). It is predicted that the MEMS market could reach more than $34 billion by the year 2002. Today, commercially available MEMS products include inkjet printer heads and accelerometers for airbags. These products require little or no assembly because a monolithic integrated circuit process is used to develop the devices. However, future MEMS products may not be so fortunate. Monolithic integration is not feasible when incompatible processes, complex geometry, or different materials are involved. For these cases, new and extremely precise micromanipulation capabilities will be required for successful product realization.

The robotics community has been investigating the technical issues associated with micromanipulation. At this point, most precision assembly is performed using teleoperated robotic systems. For example, Miyazaki [1] and Kayono [2] meticulously picked up 35 polymer particles (each 2 microns in diameter) and stacked them inside a scanning electron microscope (SEM). Mitsuishi [3] developed a teleoperated, force-reflecting, micromachining system under a SEM. On a larger scale, Zesch [4] used a vacuum gripper to pick up 100-micron diamond crystals and deposit them to arbitrary locations. Sulzmann [5] teleoperated a microrobot using 3D computer graphics (virtual reality) as the user interface.

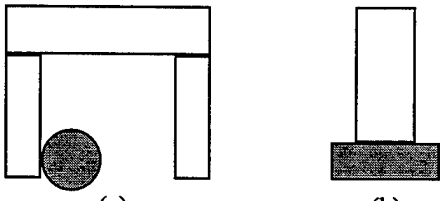

Figure 1. Micro domain problems: (a) Part adheres to one finger when the gripper opens. (b) Pneumatic probes require reversible pressure to "blow" the part away from the probe, thus releasing it.

As discussed by [6][7], the relative importance of the interactive forces in microassembly is very different from that in the macro world. Gravity is almost negligible, while surface adhesion, electrostatic, and van der Waals forces dominate. Figure 1 illustrates typical problems associated with manipulation in the micro domain. It is typically

[1] Sandia is a multiprogram laboratory operated by Sandia Corporation, a Lockheed Martin Company, for the United States Department of Energy under contract DE-AC04-94AL85000.

easy to pick up parts, but very difficult to release parts because of these interactive forces. To some extent these problems can be reduced by cleaning parts and grounding contact surfaces. It may even be possible to design the microgrippers such that these forces are reduced [6]. But these forces can not be neglected, and an assembly plan must take these effects into account.

In the "lights out" micro-machine factory of the future, an engineer would develop a set of part and assembly models in a CAD package, and a computer program would generate the required tooling, fixturing, assembly sequence, path plan, and fine motion control parameters. Figure 2 shows the elements of a simple planning system. Bidirectional arrows are used to denote feedback between the elements. This feedback may be implemented as iterative trials from the search space of the task. More complex planning systems may have more interconnects between elements, but for simplicity of illustration Figure 2 will suffice. After the engineer designs the components and subassemblies, end-effectors and fixtures would be designed and then tested by an assembly planning module which would test geometric constraints between the components, end-effectors, and fixtures. The resulting assembly plan would be passed to a fine motion planning module which would modify the goal regions based on limitations in sensing and control. Finally, this modified motion plan would be sent to a motion planning module which would generate the final gross motions between goal and pre-image regions while avoiding obstacles in the environment.

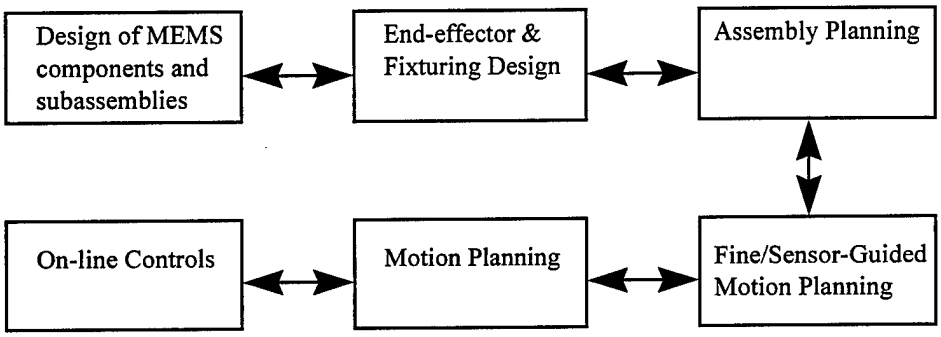

Figure 2. Flow diagram of planning system for automated assembly of MEMS.

Much research has been performed in assembly and path planning for the macro world [18], and it would be beneficial to directly apply this research where possible. In fact, the same flow diagram used in Figure 2 applies to the macro-world. So which elements need to be modified for the micro-domain? We believe that the assembly and motion planning modules in Figure 2 are unchanged in the micro-domain. The geometric constraints of the assembly planner will apply to the micro-domain as well as the free space path planning of the motion planner. However, fine motion planning and precise motion will differ from the macro-world cases, particularly when contact is involved. For example, the interactive forces in the micro-domain cause an assembly sequence not to be reversible. As pointed out in [1] (see Figure 3), reversing the motion used to pick up a part will generally not release it. The specification of goals is different and must be correctly modeled. In this paper, we investigate how motion planning changes based on the interactive forces in the micro-domain.

In the next section, we provide background on the interactive forces which affect fine motion planning in the micro-domain. The following section uses these results to automatically generate a fine motion plan which is similar to that which was generated by a human operator in [1]. The paper concludes with remarks and suggestions for future research.

DISCLAIMER

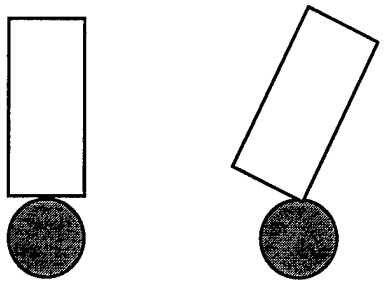

Figure 3. In [1], the blunt end of a gold plated probe was used to pick up 2 micron diameter polymer particles and stack them inside an SEM. To release the particles, the probe was moved so that the edge of the probe contacted the particle, thus decreasing the contact area and reducing attractive forces.

2. Interactive Forces

In this section, we describe two dominant interactive forces in the micro-domain: van der Waals and electrostatic. As mentioned in [6][7], surface tension also plays a dominant role in non-clean-room environments. In this paper, we will assume that the parts to be assembled are clean and that the humidity is low enough that surface tension effects can be neglected.

Throughout this section, we will consider the forces between a sphere and a rectangular block of different dimensions. The sphere represents the object being picked up, and the block represents the tool used to pick up the object. Previous works [6][7][8] have typically only considered the interactions between two spheres or between a sphere and an infinite half space. Unfortunately, these simple models can not be used to explain the motion sequence demonstrated in [1][2], where a tilting of the tool during part release is used to reduce the attractive forces to the object. In this paper, we strive to understand how to model this interaction and how this model can be used to plan assembly motions.

2.1. Van der Waals Force

Van der Waals (sometimes called London's or dispersion) force is caused by a momentary dipole moment between atoms resulting from interaction between electrons in the outermost bands rotating around the nucleus. This moment exists even for atoms which do not contain a permanent polarization. While the average distribution of electrons is uniformly distributed about the nucleus, the outermost electrons of one atom are inducing a dipole on the other atoms which in turn induce a dipole on still more atoms. An easy-to-read overview of van der Waals forces is given in [9].

The end result is that the interaction energy between two atoms or molecules is proportional to the inverse of the sixth power of distance between the molecules.

$$E_i = -\frac{\lambda}{r^6} \tag{1}$$

where r is the distance between the molecule centers and λ is a constant. This constant depends on temperature and material properties such as the distortion polarization, permanent dipole moment, and ionization energy.

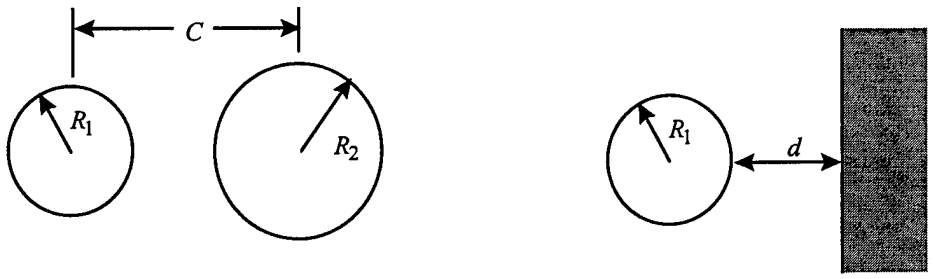

(a) (b)

Figure 4. Notation for (a) two spheres, (b) sphere and half space.

Hamaker [10] computed the non-retarded interaction energy and force between two macroscopic spheres (see Figure 4a). The energy of interaction between two particles containing n atoms per cm^3 is given by

$$E = -\int_{V_1}\int_{V_2} \frac{n^2\lambda}{r^6} dv_2\, dv_1 \tag{2}$$

where V_1 and V_2 are the volumes of the first and second particles. Integrating the volume of two spheres, Hamaker found that the energy is given by

$$E_{vdwoo} = \frac{-H}{12}\left[\frac{R_1R_2}{C^2-(R_1+R_2)^2} + \frac{R_1R_2}{C^2-(R_1-R_2)^2} + 2\ln\frac{C^2-(R_1+R_2)^2}{C^2-(R_1-R_2)^2}\right] \tag{3}$$

where R_1 and R_2 are the radii of the two spheres, C is the distance between centers, and $H = \pi^2 n^2 \lambda$ is the Hamaker constant. The subscript *vdwoo* stands for van der Waal between two spheres. The corresponding force between two spheres is determined by taking the partial derivative with respect to C.

$$F_{vdwoo} = \frac{HCR_1R_2}{3}\left[\frac{8R_1^2R_2^2 - \left[C^2-(R_1-R_2)^2\right]\left[C^2-(R_1+R_2)^2\right]}{\left[C^2-(R_1+R_2)^2\right]^2\left[C^2-(R_1-R_2)^2\right]^2}\right] \tag{4}$$

By letting R_2 go to infinity, Hamaker also determined the non-retarded energy between a sphere and an infinite half space. It is given by

$$E_{vdwo|} = \frac{-H}{6}\left[\frac{R_1}{d} + \frac{R_1}{d+2R_1} + \ln\frac{d}{d+2R_1}\right] \tag{5}$$

where d is the distance from the wall to the edge of the sphere. The subscript *vdwo|* stands for van der Waal between a sphere and a half space. The corresponding force is

$$F_{vdwo|} = \frac{2HR_1^3}{3d^2(d+2R_1)^2} \tag{6}$$

As pointed out in [16], the energy of the approximation (1) changes from an inverse sixth to an inverse seventh power law at separations greater than 10nm to 50nm. This retardation is explained when accounting for the time of travel of the polarization field as it travels from one atom to the next. As the distance increases, the time of travel approaches the lifetime of the instantaneous dipole of the original molecule. Instead of the induced fields being additive, they become subtractive, and the energy and force of interaction is reduced. Lifshitz [11] first explained this phenomena, and others have gone on to develop very detailed (and computationally intensive) models which include this "screening" effect between dipoles [12-15].

While these more detailed models are more accurate, they are difficult to compute for more complex particle shapes. Therefore, in this paper we have chosen to compute the non-retarded energy and force between a sphere and a rectangular block. This provides an upper bound on the interaction forces which will exist in experimentation. More importantly, this upper bound gives us a qualitative feel for how van der Waals forces affects motion planning as described in the next section.

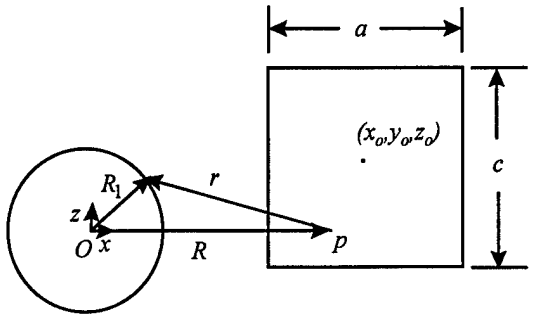

Figure 5. Notation for computing van der Waals energy between a sphere of radius R_1 and a rectangular block centered at (x_O, y_O, z_O) and of dimensions (a, b, c). The y direction at origin O is into the page.

The derivation of energy between a sphere and a rectangular block follows that of Hamaker [10]. The energy of a particle p outside of the sphere is determined by integrating van der Waals energy inside the volume of the sphere with respect to the coordinates of p (see Figure 5).

$$E_p = -\int_{R-R_1}^{R+R_1} \frac{\pi\lambda n}{Rr^5}\left(R_1^2 - (R-r)^2\right)dr$$
$$= \frac{-\pi\lambda n}{12R}\left[\frac{2R_1}{(R+R_1)^3} + \frac{2R_1}{(R-R_1)^3} + \frac{1}{(R+R_1)^2} - \frac{1}{(R-R_1)^2}\right] \quad (7)$$

where R_1 is the radius of the sphere and R is the distance from the center of the sphere to particle p. For a 2 micron diameter copper sphere, E_p changes versus distance (either radial or tangential) as shown in Figure 6. Notice how energy decreases drastically versus radial distance as compared to the tangential distance. The same decrease in energy is seen over a radial change of 10 Angstroms as is seen over a tangential change of 1000 Angstroms.

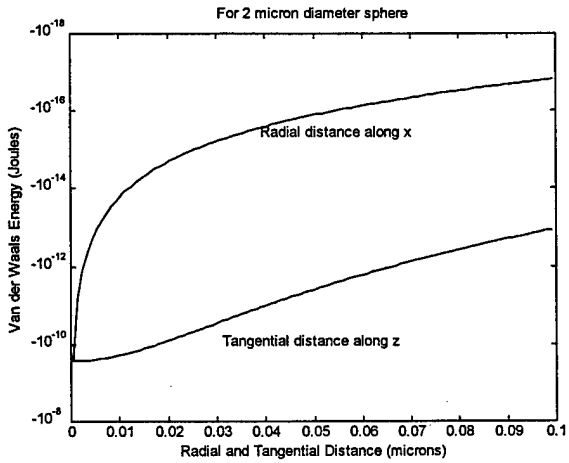

Figure 6. Van der Waals energy between a 2 micron diameter copper sphere and a copper atom. Hamaker's constant for copper is 32.4676×10^{-20} J. The minimum distance between the sphere and the atom is 4 Angstroms.

The total energy between the sphere and a block is determined by integrating E_p inside the block's rectangular volume.

$$E_{vdwob} = \int_{z_o-c/2}^{z_o+c/2}\int_{y_o-b/2}^{y_o+b/2}\int_{x_o-a/2}^{x_o+a/2} E_p n \, dx \, dy \, dz \tag{8}$$

where

$$R = \sqrt{x^2 + y^2 + z^2} \, .$$

The subscript *vdwob* stands for van der Waal between a sphere and a block. This expression is a difficult integral to evaluate symbolically, so we have opted to evaluate it numerically using Gauss-Legendre integration. Using 40 abscissa points, this integration is exact for all polynomials of degree 79 or less. The van der Waals force along the x, y, and z axis is given by

$$F_l = \frac{\partial F}{\partial l} = \int_{z_o-c/2}^{z_o+c/2}\int_{y_o-b/2}^{y_o+b/2}\int_{x_o-a/2}^{x_o+a/2} \frac{\partial E_p}{\partial R}\frac{\partial R}{\partial l} n \, dx \, dy \, dz, \quad l = x, y, z \tag{9}$$

where

$$\frac{\partial E_p}{\partial R} = \frac{\pi\lambda n}{4R^2}\left[\frac{2RR_1}{(R+R_1)^4} + \frac{2RR_1}{(R-R_1)^4} + \frac{1}{(R+R_1)^2} - \frac{1}{(R-R_1)^2}\right] \quad \text{and} \quad \frac{\partial R}{\partial l} = \frac{l}{R}.$$

This triple integral is also computed numerically using Gauss-Legendre integration.

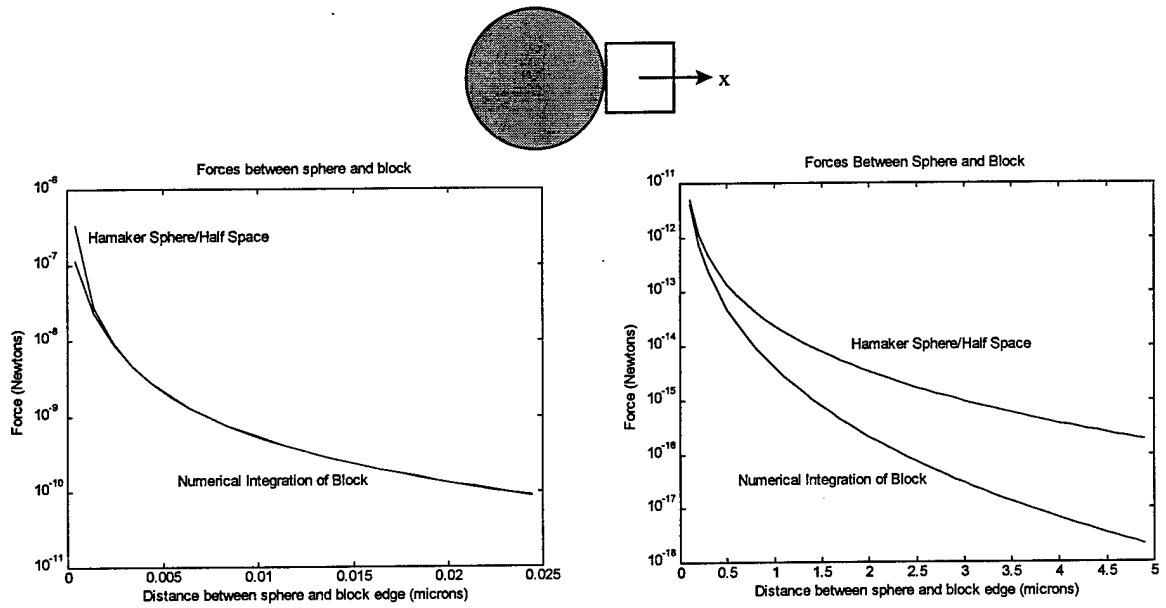

Figure 7. Van der Waals force between a 2 micron diameter copper sphere and a 1 μm^3 copper rectangular block as the block is moved radially away from the sphere. For copper, the Hamaker constant is H=32.4676x10^{-20} Joules.

Figure 7 shows the van der Waals force between a 2 micron diameter copper sphere and a 1 μm^3 copper block as the block moves away from the sphere in the x direction. As a comparison, the van der Waals force between a sphere and a half space as given in Equation (6) is also shown. Note that the van der Waals force between the sphere and

block is less than that between a sphere and half space when the two objects are touching. As the block moves away from the sphere, the sphere/half space and sphere/block forces are approximately equal when the objects are very close. As the block moves further away, the van der Waals forces for the sphere/block are less than for the sphere/half space. These results are intuitively correct. It should also be noted that the gravitational force on a 2 micron diameter sphere of copper is 3.678093×10^{-13} N. So the van der Waals force is the dominant force for separations less than 0.5 microns.

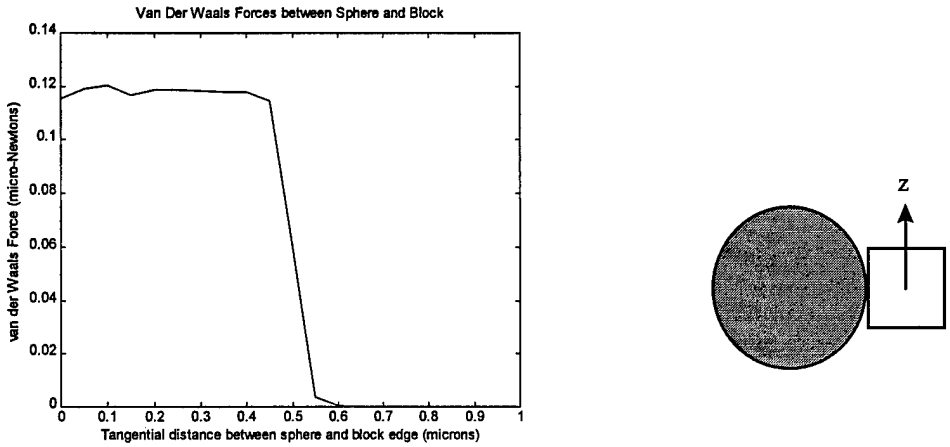

Figure 8. Van der Waals force between a 2 micron diameter copper sphere and a 1 μm^3 copper rectangular block as the block is moved tangentially away from the sphere.

Figure 8 shows the van der Waals force between the sphere and the block as the block is translated tangentially to the sphere in the *z* direction. Notice that the force remains relatively constant until the corner of the block reaches the edge of the sphere. At this point the force is one-half of the force when the block is centered on the sphere. As the block moves further along the tangential direction, the force decreases dramatically since the block is no longer in contact with the sphere.

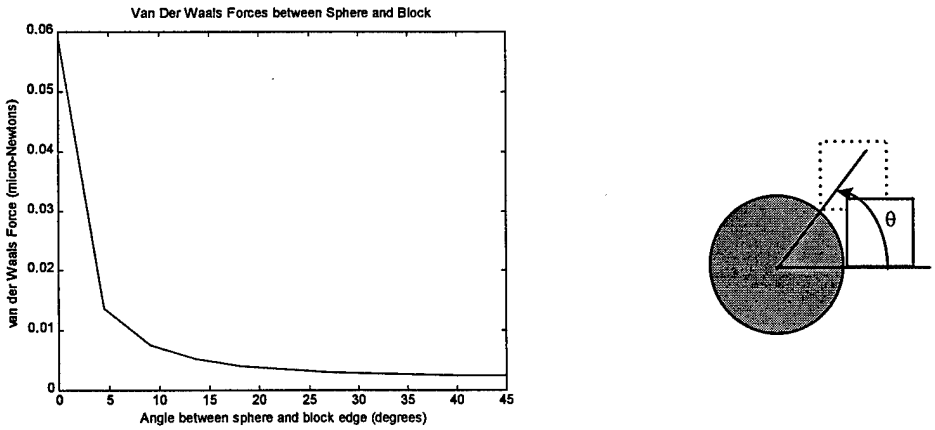

Figure 9. Van der Waals force between a 2 micron diameter copper sphere and a 1 μm^3 copper rectangular block as the block is rotated around the sphere.

Figure 9 shows the van der Waals force between the sphere and the block as the block is rotated with respect to the sphere. This is computed by moving the block in the x and z directions simultaneously so that a corner of the block is always touching the sphere (4 Angstroms away). Again, the force of interaction drops off as the block rotates to

45 degrees. From Figures 8-9, we can see that the minimum in-contact van der Waals force occurs when the block is touching the sphere on it's edge at 45 degrees. Because van der Waals force is very short range, this position of minimum in-contact force changes very little as the dimensions of the block change. As will be seen in the path planning section, this position of minimum in-contact force may be used to plan the release position of a grasp.

2.2 Electrostatic Force

Now let us look at the second interactive force: electrostatic. We will only consider the electrostatic force between two conducting particles with a thin dielectric layer to insulate the two. As pointed out in [7], dielectric oxide layers of up to 1nm are possible after several days in air at room temperature. Again, we will compute the forces between a sphere and a rectangular block.

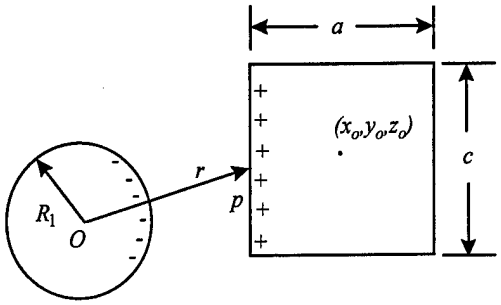

Figure 10. Notation for computing electrostatic force between a sphere of radius R_1 and a rectangular block centered at (x_O, y_O, z_O) and of dimensions (a, b, c). The y direction at origin O is into the page.

For a conductor, the electric field inside of the sphere and the block will be zero, and all electrostatic charge will reside on the surface (see Figure 10). Using Gauss's law, it can be shown that the electric field between a particle p and the sphere is given by [16]

$$\vec{E}_1 = \frac{Q_1}{4\pi\varepsilon_o r^2}\hat{r}, \quad r > R_1 \tag{10}$$

where

$$r^2 = x^2 + y^2 + z^2$$

$$Q_1 = 4\pi R_1^2 \sigma_1$$

r is the distance from the center of the sphere to the particle, $\hat{r}$ is the unit vector from the center of the sphere to the particle, R_1 is the radius of the sphere, σ_1 is the charge density of the sphere, and ε_o is the permittivity of air ($8.85\text{x}10^{-12}$ $C^2/(Nm^2)$). The infinitesimal force on a charge on the block's surface is given by

$$d\vec{F} = \vec{E}_1 \sigma_2 da_2 \tag{11}$$

where σ_2 is the charge density of the block and da_2 is the infinitesimal area of the block's surface. The force in the x direction on the side of the block closest to the sphere (see Figure 10) is

$$\begin{aligned} F_x\big|_{x=x_o-a/2} &= \int_{z_o-c/2}^{z_o+c/2}\int_{y_o-b/2}^{y_o+b/2} \sigma_2 E_1\big|_{x=x_o-a/2} \frac{x_o - a/2}{\sqrt{\left(x_o - a/2\right)^2 + y^2 + z^2}}\, dydz \\ &= \frac{R_1^2 \sigma_1 \sigma_2 \left(x_o - a/2\right)}{\varepsilon_o} \int_{z_o-c/2}^{z_o+c/2}\int_{y_o-b/2}^{y_o+b/2} \frac{1}{\left[\left(x_o - a/2\right)^2 + y^2 + z^2\right]^{3/2}}\, dydz \end{aligned} \tag{12}$$

Similarly, the forces in the y and z directions on the side closest to the sphere are

$$F_y\Big|_{x=x_o-a/2} = \frac{R_1^2\sigma_1\sigma_2}{\varepsilon_o}\int_{z_o-c/2}^{z_o+c/2}\int_{y_o-b/2}^{y_o+b/2}\frac{y}{\left[\left(x_o-a/2\right)^2+y^2+z^2\right]^{3/2}}dydz \tag{13}$$

$$F_z\Big|_{x=x_o-a/2} = \frac{R_1^2\sigma_1\sigma_2}{\varepsilon_o}\int_{z_o-c/2}^{z_o+c/2}\int_{y_o-b/2}^{y_o+b/2}\frac{z}{\left[\left(x_o-a/2\right)^2+y^2+z^2\right]^{3/2}}dydz \tag{14}$$

In these expressions, the inner integral can easily be integrated analytically, but the outer integral is more complex, so it has been computed numerically. Similar expressions can be found for the forces exerted on the other five sides of the block. The total forces are given by

$$F_l = F_l\Big|_{x=x_o-a/2} + F_l\Big|_{x=x_o+a/2} + F_l\Big|_{y=y_o-b/2} + F_l\Big|_{y=y_o+b/2} + F_l\Big|_{z=z_o-c/2} + F_l\Big|_{z=z_o+c/2} \quad , \quad l = x, y, z \tag{15}$$

Figures 11 and 12 show the force of electrostatic attraction for a 2 micron diameter sphere and a 1 μm^3 rectangular block, both with surface charge densities of $25x10^{-6}$ C/m^2. As reported in [2], the breakdown strength of air is limited to a maximum charge density of about $30x10^{-6}$ C/m^2 at atmospheric pressure. As the block moves away from the sphere in the x and z directions, the electrostatic force decreases. Because of symmetry, the force in the y direction is zero. Notice that the electrostatic force does not drop off as quickly as the van der Waals forces. This is because the electrostatic force is a longer range force. Figure 13 shows the electrostatic force as the block is rotated with respect to the sphere. Again, the force of interaction drops off as the block rotates to 45 degrees. Similar to van der Waals forces, the minimum in-contact force occurs when the edge of the block is at 45 degrees to the sphere. However, since electrostatics is a longer range force, the minimum in-contact force is not at 45 degrees if the dimensions of the block change. For example, if the x dimension (a) is larger than the z dimension (c), then the minimum in-contact force will occur at less than 45 degrees.

These results will be used in the next section to determine the goal regions for picking up and releasing a sphere with a rectangular block gripper.

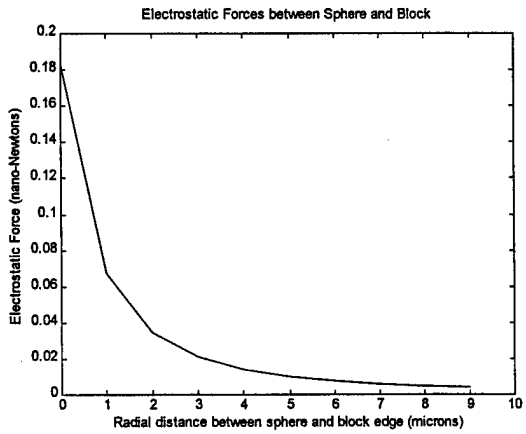

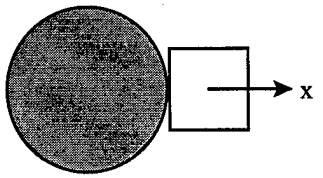

Figure 11. Electrostatic force between a 2 micron diameter sphere and a 1 μm^3 rectangular block as the block is moved radially away from the sphere. The surface charge density of both the sphere and block are $25x10^{-6}$ C/m^2. Minimum separation is 4 Angstroms.

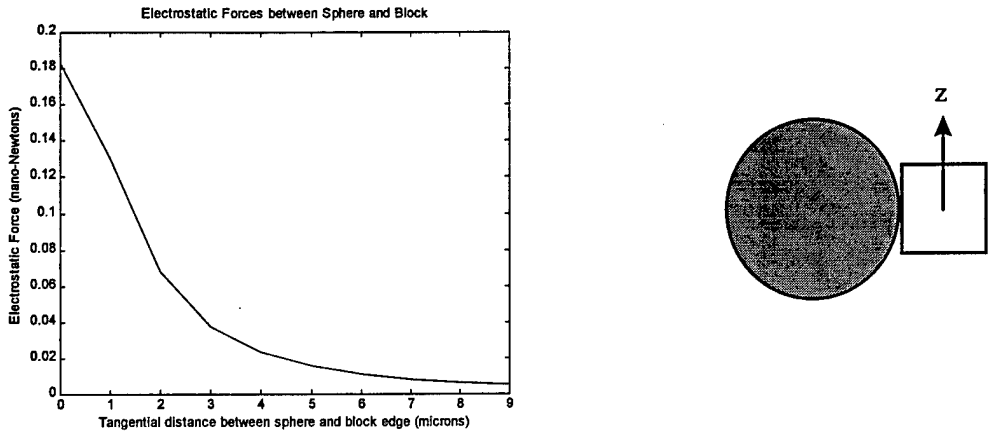

Figure 12. Electrostatic force between a 2 micron diameter copper sphere and a 1 μm^3 copper rectangular block as the block is moved tangentially away from the sphere. Minimum separation in the x direction is 4 Angstroms.

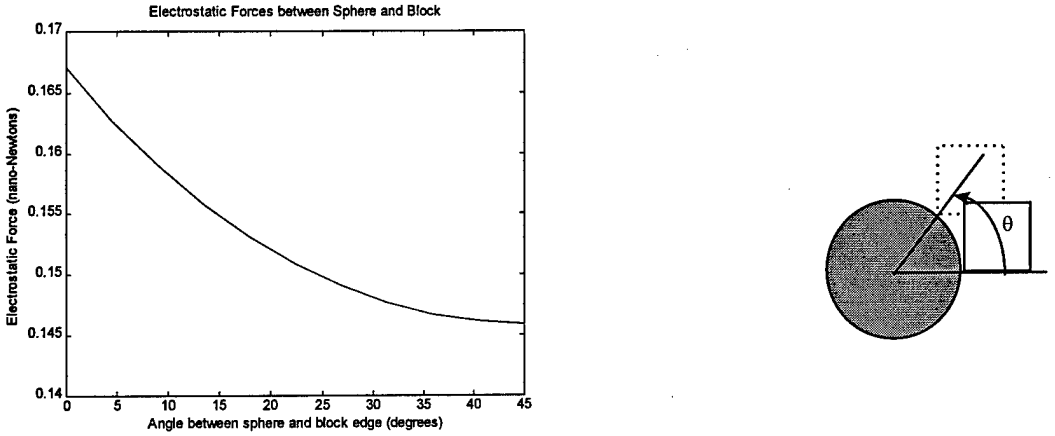

Figure 13. Electrostatic force between a 2 micron diameter copper sphere and a 1 μm^3 copper rectangular block as the block is rotated around the sphere. Minimum separation is 4 Angstroms.

3. Path Planning

Considerable research has been performed in motion planning and is summarized in [18]. As mentioned in the introduction, we believe that much of the work developed for the macro-world will directly apply to the micro-domain except where performing fine motion control. One example where macro-world fine motion planning is not acceptable in the micro-domain is compliant motion. While [19-22] showed that compliant motion may be used to expand the acceptable motion control uncertainty for peg-in-hole insertions and other placement tasks in the macro-world, this is not desirable in the micro-domain. First, compliant motion in the micro-domain generates particles on the rubbing surfaces which further complicate the assembly. Second, the friction cone on micro-surfaces will be enlarged because of the dominant van der Waals and electrostatic forces mentioned in the previous sections.

Another example of where macro-world fine motion planning needs to be modified for the micro-domain is fine motion vision planning as described in [23]. In the macro-world, simple geometric optics have been used for fine motion planning where vision is used as a feedback sensor. In the micro-domain, the size of the parts approach the wavelength of light, and complex nonlinear optics is needed to predict the effects of Fraunhoffer diffraction on the

image processing [24]. This result will require that all fine motion control must occur in the very narrow depth of field of the microscope optics. This is an area of future research.

In this section, we will investigate how the force relationships presented in the previous section affects fine motion planning with force sensing. In particular, we will concentrate on the simple pick-up and release of a spherical particle with a rectangular block shaped tool. For simplicity, we will only consider motion planning in the x, z, and θ space as shown in Figure 14.

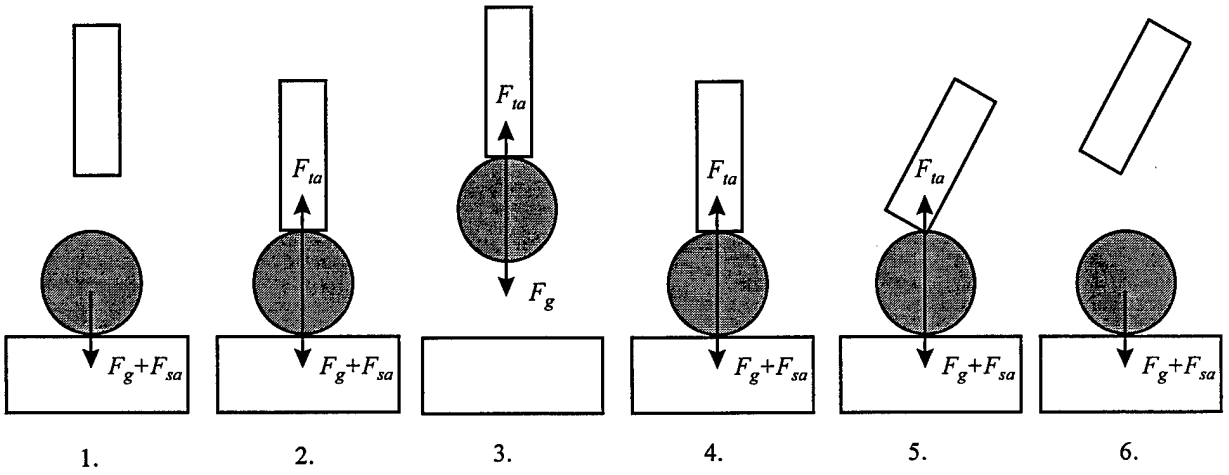

Figure 14. Steps to pick up and release a sphere with a flat-tipped tool assuming only van der Waals forces and no electrostatic forces. Between steps 4 and 5, a rolling contact is assumed.

The static forces acting on the sphere at the various stages of pick up and release are the force of gravity F_g, the force of surface attraction F_{sa}, and the force of tool attraction F_{ta}. To pick up the part, the force of tool attraction must be greater than the gravitational force and the force of surface attraction. To hold the part, the force of tool attraction must be greater than the gravitational force. Finally, to release the part, the force of tool attraction must be less than the gravitational force and the force of surface attraction. In summary,

$$\begin{aligned} F_{ta} &> F_g + F_{sa} && \text{to pick up part} \\ F_{ta} &> F_g && \text{while holding part} \\ F_{ta} &< F_g + F_{sa} && \text{to release part} \end{aligned} \tag{16}$$

For ease of illustration, assume that both the sphere and the tool tip are made of copper, and there is no electrical charge on either the sphere, tool, or assembly surface. In other words, electrostatic forces are negligible. Initially, the sphere is resting on a surface of a different material. If the resting surface were also of copper, we would not be able to pick up the sphere with a flat tipped tool. The force of gravity acting on the sphere is given by

$$F_g = \frac{4}{3}\pi R_1^3 \rho g \tag{17}$$

where R_1 is the radius of the sphere, ρ is the density of the material, and g is the gravitational acceleration. For a 2 micron diameter sphere of copper, $F_g = 3.678093\text{x}10^{-13}$ N. The force of attraction between the sphere and the surface is given by Equation (6). In certain cases, the equivalent Hamaker constant for two different materials is given by

$$H_{12} = \sqrt{H_1 H_2} \tag{18}$$

where H_1 and H_2 are the Hamaker constants for the individual materials. If the resting surface is made of a aluminum ($H_2 = 3.43774\text{x}10^{-20}$ Joules), then the composite Hamaker constant is $H_{12} = 10.5648\text{x}10^{-20}$ Joules.

Assuming a 4 Angstrom separation and the same 2 micron diameter copper sphere considered in the previous section, the van der Waals force between the copper sphere and the aluminum surface is $F_{sa} = 0.110$ μN. Assuming that the tool has the same dimensions as the 1 μm^3 copper block considered in the previous section, the force of tool attraction is $F_{ta} = 0.116$ μN when the tool is centered over the sphere. When the tool is moved so that one edge is on the surface of the sphere, the force of tool attraction becomes $F_{ta} = 0.059$ μN. When the tool is tilted at 45 degrees, the force of tool attraction decreases to $F_{ta} = 0.025$ μN.

For the values of F_{ta}, F_g, *and* F_{sa} mentioned above, the tool will be able to pick up the sphere by centering the tool over the sphere. As seen in Figure 8, the force of tip attraction stays fairly constant over the width of the tip (approximately 1 μm). Because the gravitational forces are so small, the tool will be able to hold the sphere even when in the minimum in-contact position (the edge of the probe is at 45 degrees to the sphere). To release the sphere, the tool must be moved to the edge of the sphere. In this particular case, the tool will not have to be tilted to further reduce F_{ta}. In other cases where the surface material changes or the size of the sphere and tool change, the tool may have to be tilted to further reduce F_{ta}.

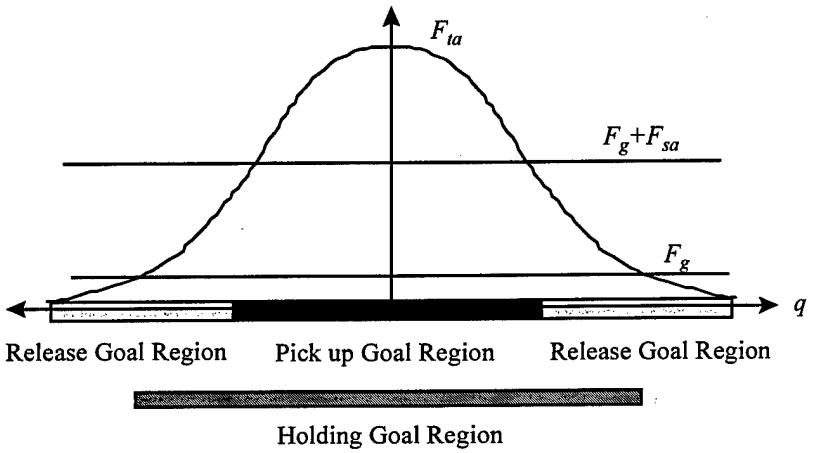

Figure 15. Release, pick up, and holding goal regions in configuration space are determined from the interactive forces in the micro-domain.

In general, Equation (16) together with the equations for attractive forces described in the previous section can be used to classify the various goal regions in configuration space [25]. Once the pick-up, holding, and release goal regions are determined, normal assembly and path planning routines can be used to determine assembly sequences and collision-free path plans. Figure 15 shows a one-dimensional plot of attractive tool force versus the configuration q. In the example above, configuration q is a three-dimensional space including the x and z position and orientation of the tool. A planning routine must search this space while the tool contacts the part and classify the goal regions using Equation (16). This search is not as difficult as it first appears since the dimension of the search space is greatly reduced by the in-contact (within say 4 Angstroms) constraint between the tool and the part. If the user-specified goal region of the sphere is chosen to be a single point on the arc and the user-specified goal region on the tool is the bottom line segment excluding the end points (see Figure 16a), then the search space reduces to a 1 dimensional search along a tangent line segment (as was performed in Figure 8). The line segment of the tool must be tangent to the sphere at the user-specified goal point on the sphere; otherwise, the tool will penetrate the sphere.

If the end points of the tool edge are included in the user-specified goal region on the tool, the tool may freely rotate about the end-point where the tool contacts the sphere. The range of rotation is 180 degrees minus the angle between the tool goal region and the adjacent line segment of the tool. With the end-points are included, a 1 dimensional rotational search at both end-points will be required as shown in Figure 9. The time complexity of the problem is $O(n+2m)$ where n is the discretization along the tool line segment and m is the discretization in angular rotation at the end-points.

The dimensions of the search space increase if the user-specified goal region on the sphere is an arc segment instead of a single point (see Figure 16b). The time complexity of the problem becomes $O(n^2+2mn)$ where the same discretization n is used along the arc of the sphere and the line segment of the tool.

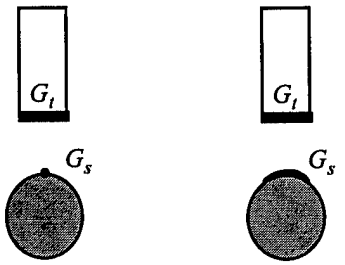

Figure 16. User-specified goal regions on the tool G_t and on the sphere G_S. User-specified goal region on the tool is a line segment. (a) User-specified goal region on the sphere is a single point. (b) User-specified goal region on the sphere is an arc.

4. Conclusions

In this paper, we took the first steps in explaining how to approach assembly planning in the micro-domain. We believe that free-space motion planning and the geometric assembly constraints in macro-world planners will directly apply to the micro-domain. However, fine motion planning and precise motion will differ from the macro-world. In particular, we have shown that van der Waals and electrostatic forces will alter the goal regions for pick-up, hold, and release tasks. In this paper, we developed the mathematics necessary to locate these goal regions for a spherical part being manipulated by a rectangular block. We are currently in the process of developing a pre-planner which will search configuration space when a tool contacts a part to determine the acceptable goal regions for pick-up, holding, and release of a part.

Since this is a new area of research, much work still needs to be performed. Our future plans are to look at more complex part and tool shapes. Evaluation of van der Waals and electrostatic forces will become significantly more difficult as we investigate shapes other than spheres and rectangular blocks. Finite element models [17] will be required to compute the forces between these more complex shapes. Once the goal regions are specified, realistic termination predicates using force, time, and vision as sensing modalities need to be specified. Instrumentation that can measure sub-micro-Newtons of force needs to be developed. Fine motion planning using visual constraints [23] that have been modified by diffraction effects [24] at the micro-scale is also an area of research. Finally, how these goal regions affect planning under uncertainty needs to be addressed.

References

[1] H. Miyazaki, T. Sato, "Pick and Place Shape Forming of Three-Dimensional Micro Structures from Fine Particles," *Proc. of ICRA 1996*, pp. 2535-2540.
[2] K. Koyano, T. Sato, "Micro Object handling System with Concentrated Visual Fields and New Handling Skills," *Proc. of ICRA 1996*, pp. 2541-2548.
[3] M. Mitsuishi, N. Sugita, T. Nagao, Y. Hatamura, "A Tele-Micro Machining System with Operation Environment Transmission under a Stereo-SEM," *Proc. of ICRA 1996*, pp. 2194-2201.
[4] W. Zesch, M. Brunner, A. Weber, "Vacuum Tool for Handling Microobjects with a Nanorobot," *Proc. of ICRA 1997*, pp. 1761-1766.

[5] A. Sulzmann, H.-M. Breguett, J. Jacot, "Microvision system (MVS): a 3D Computer Graphic-Based Microrobt telemanipulation and Position Feedback by Vision," *Proc. of SPIE Vol. 2593*, Philadelphia, Oct. 25, 1995.
[6] R. Arai, D. Ando, T. Fukuda, Y. Nonoda, T. Oota, "Micro Manipulation Based on Micro Physics - Strategy Based on Attractive Force Reduction and Stress Measurement," *Proc. of ICRA 1995*, pp. 236-241.
[7] R.S. Fearing, "Survey of Sticking Effects for Micro Parts Handling," *Proc. of IROS '95*, Pittsburgh, PA, August 1995, Vol. 2, pp. 212-217.
[8] R. Allen Bowling, "A Theoretical Review of Particle Adhesion," *Particles on Surfaces 1*, K.L. Mittal, editor, pp. 129-142, 1988.
[9] J.N Israelachvili, "The Nature of van der Waals Forces," *Contemporary Physics*, Vol. 15, No. 2, pp. 159-177, 1974.
[10] H.C. Hamaker, "The London-van der Waals Attraction Between Spherical Particles," *Physica IV*, No. 10, pp. 1058-1072, November 1937.
[11] E.M. Lifshitz, Sov. Phys. JETP, Vol. 2, 73, 1956.
[12] D. Langbein, "Non-Retarded Dispersion Energy Between Macroscopic Spheres," *J. Phys. Chem. Solids*, Vol. 32, pp. 1657-1667, 1971.
[13] D. Langbein, *Theory of Van der Waals Attraction*, Springer Tracts in Modern Physics, 1974.
[14] J.E. Kiefer, V.A. Parsegian, and G.H. Weiss, "Some Convenient Bounds and Approximations for the Many Body Van der Waals Attraction between Two Spheres," *J. Colloid and Interface Science*, Vol. 67, No. 1, pp. 140-153, October 1978.
[15] H.W. Marlow, "Survey of Aerosol Interaction Forces," *Aerosol Microphysics I*, W.H. Marlow, editor, pp. 117-156, 1980.
[16] N.H. Nayfeh, M.K. Brussel, *Electricity and Magnetism*, 1985.
[17] D. McAllister, J.R. Smith, and N.J. Diserens, *Computer Modelling in Electrostatics*, 1985.
[18] J.-C. Latombe, *Robot Motion Planning*, 1991.
[19] T. Lozano-Perez, M.T. Mason, R.H. Taylor, "Automatic Synthesis of Fine-Motion Strategies for Robots," *The International Journal of Robotics Research*, Vol. 3, No. 1, pp. 3-24, Spring 1984.
[20] M.A. Erdmann. "Using Backprojections for Fine Motion Planning with Uncertainty," *International Journal of Robotics Research*, Vol. 5, No. 1, Spring 1986.
[21] B.R. Donald, "A Geometric Approach to Error Detection and Recovery for Robot Motion Planning with Uncertainty," *Artificial Intelligence*, Vol. 37, 1988.
[22] J. -C. Latombe, "Motion Planning with Uncertainty: On the Preimage Backchaining Approach," *The Robotics Review I*, O. Khatib, et al, editors, MIT Press, 1989.
[23] A. Fox and S. Hutchenson, "Exploiting Visual Constraints in the Synthesis of Uncertainty-Tolerant Motion Plans," *IEEE Transactions on Robotics and Automation*, Vol. 11, No. 1, pp. 56-71, February 1995.
[24] J.T. Feddema, R.W. Simon, "CAD-Driven Microassembly and Visual Servoing," *Proc. 1998 IEEE International Conference on Robotics and Automation*, Belgium, May 16-21, 1998.
[25] T. Lozano-Perez, "Spatial Planning: A Configuration Space Approach," *IEEE Transactions on Computers*, Vol. C-32, No. 2, pp. 108-120, February 1983.

Report Number (14) SAND--98-0896C
CONF-980537--

Publ. Date (11) 19980516
Sponsor Code (18) DOE/ER, XF
UC Category (19) UC-900, DOE/ER

DOE